Reproducible interconnects assembled from gold nanorods

Birol Ozturk, Charles Blackledge, and Bret N. Flanders[a)]
Department of Physics, Oklahoma State University, Stillwater, Oklahoma 74078

Daniel R. Grischkowsky
School of Electrical and Computer Engineering, Oklahoma State University, Stillwater, Oklahoma 74078

(Received 10 June 2005; accepted 3 January 2006; published online 15 February 2006)

By using cleanroom-based lithographic procedures to produce identical electrode arrays, we have fabricated dielectrophoretic nanowires that vary in their conductance by ±10%. Transmission electron microscopy established the presence of interconnect segments composed of densely aggregated nanoparticles and of individual nanorods lying in the current-carrying path. The current-voltage profiles of these interconnects exhibited barriers to charge transport at temperatures less than ~225 K; furthermore, their conductances increased exponentially with temperature with an activation energy comparable to the nanorod charging energy. These results indicate that the Coulomb blockade associated with individual nanorods in the interconnects is the primary conductance-limiting feature. © *2006 American Institute of Physics*. [DOI: 10.1063/1.2174109]

Dielectrophoretic assembly has emerged as a promising approach to in-parallel device fabrication that exploits the spontaneous behavior of building block populations. In dielectrophoretic assembly, the dipolar term of the interparticle potential of a colloidal dispersion is amplified, leading to the single-step assembly and interfacing of electrical interconnects with surrounding circuitry.[1,2] Several groups have used this approach to integrate nanowires, nanoparticles, and interconnects with existing electronics.[2–5] Because of the lack of reproducibility in the fabrication conditions of individually fabricated samples, there have been relatively few detailed investigations of the charge-transport properties of dielectrophoretic interconnects.[3]

Here, we have employed standard photolithography to fabricate sets of identical electrode pairs on 500 μm thick quartz substrates, eliminating much of the nonuniformity that hampers wire-by-wire assembly and enabling the simultaneous fabrication of up to six interconnects under identical growth conditions (electrode-geometry, voltage amplitude and frequency, and concentration of nanoparticle solution). Figure 1(a) depicts the simple circuit that facilitates the targeted placement of reproducible interconnects. An optical micrograph depicts the three electrode pairs, between which three simultaneously grown interconnects span the 100 μm gaps. The initial metal layer on these substrates was 100 nm of Ti onto which 500 nm of Al was deposited.

We have previously demonstrated the dielectrophoretic assembly of interconnects composed of 3.7 nm diameter CdS nanoparticles.[6] However, this work[6] stopped short of revealing the structural and transport properties of these interconnects because the small size of the CdS nanoparticles inhibited resolution of the mesoscopic (i.e., particle level) structure of the interconnect. To gain this knowledge, the present study employs ~30 nm gold nanorods as the building blocks, easily visible with a transmission electron microscope (TEM) of moderate resolving power. We employed an established wet chemical approach to synthesize the gold nanorods.[7,8] The resulting stock solution of nanorods contained large excesses of cetyl trimethylammonium cations and bromide anions that prevented dielectrophoretic fabrication. Hence, we centrifuged the suspensions (at 15 krpm for 20 min) to separate the nanorods from the salt solution. After resuspending the nanorods in water, this process was repeated three additional times. Figure 1(b) depicts a transmission electron micrograph of these Au nanorods, obtained by dispersing a 7 μL aliquot of the aqueous nanorod solution onto a grid and imaging the dried dispersion with the microscope (JEOL JEM 100 CX II). Analysis of five such images yielded a mean rod diameter of 10.8 nm and length of 31.2 nm.

After diluting the nanorod suspension by 10^4, a 60 μL drop is deposited across the electrode gap. The geometry of the electrodes gives rise to strong electric-field gradients upon application of a ±30 V alternating voltage. The field gradient determines the dielectrophoretic trapping force that draws the particles to the field maximum near the floating electrode. The polarizable particles become strongly dipolar under the field, inducing spontaneous chaining of neighboring particles along the interelectrode line.[1] The lower inset of Fig. 2 depicts a typical interconnect of ~140 nm diameter and 60 μm length.

The upper inset to Fig. 2 depicts dc current-voltage (*I-V*) profiles of 15 different 60 μm long interconnects that were assembled three at a time between lithographic electrodes. Fourteen of the interconnects show a linear response with measured resistances between 20 kΩ and 48 kΩ. Twelve of the interconnects have measured resistances between 27 kΩ and 41 kΩ. The dashed black line denotes the *I-V* profile of the nanorod solution in the absence of an interconnect. The average of the resistances obtained from these 60 μm long interconnects was 34 kΩ±3 kΩ, where the uncertainty is the standard error. The electrical properties of the interconnects are remarkably reproducible. By performing similar analyses on 15 samples each of 100, 220, and 500 μm long interconnects, we obtained length-dependent resistances of 113 kΩ±7 kΩ, 165 kΩ±8 kΩ, and 450 kΩ±50 kΩ, respectively. Figure 2 shows that the resistance increases linearly, indicating length-wise structural uniformity. Additionally, the linear fitting function passes

[a)]Electronic mail: bret.flanders@okstate.edu

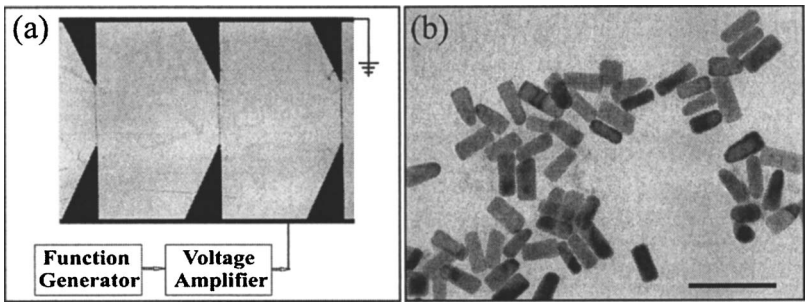

FIG. 1. (a) The electrode array consists of 120 μm wide conducting lines (resistance 1.35 Ω/mm) that extend from macroscopic contact pads (not shown) to the electrodes. The conducting lines taper across a length of 250 μm to 2 μm diameter tips. The 100–400 kHz sinusoidal output from the function generator (Hewlett Packard, HP8111A) was passed through the voltage amplifier (FLC Electronics, F10A) connected to the three electrode-pairs. (b) A transmission electron micrograph of 30 nm long and 11 nm wide Au nanorods. The scale bar represents 100 nm.

through the origin, indicating that the electrode-interconnect contact resistance is negligible.

Figure 3 depicts transmission electron micrographs of an interconnect dielectrophoretically assembled from the 30 nm long nanorods. These images were collected after transfer of the interconnect from the electrode array to a nickel grid for high-resolution imaging. The inset depicts a $\sim$10 μm segment of the interconnect, while Fig. 3 shows a more highly magnified view of the right-central portion of this segment. The interconnect is two to four nanorods wide at most points along its length, with substantial contact between the nanorods. The absence of gaps between the nanorods suggests that the assembly process induces the electromigration of gold to the regions between nanorods, effectively welding them into continuous segments significantly larger than the nanorods; however, high-resolution TEM imaging is required to substantiate this interpretation. Moreover, individual nanorods that are not tightly integrated with their neighbors are also apparent. For example, at one point along this interconnect segment, its diameter narrows to a single nanorod. In order for the current to flow, a charge must move onto this nanorod. Of course, the process of transferring the interconnect to the TEM grid may disrupt the structure of the nascent wire. Nevertheless, it is reasonable that individual unfused nanorods lie in the current-conduction path. Due to the small capacitance C of such nanorods, there is a substantial charging energy $E_c = e^2/2C$ that must be overcome in order for an electron of charge e to occupy the neutral particle.[9,10] This barrier, known as the Coulomb blockade, is estimated as follows. We approximate the nanorod capacitance by the self-capacitance of a cylinder,[11] $C = 2\pi\varepsilon\varepsilon_o \ell/\ln(\ell/r)$, where $\varepsilon_o = 8.854 \times 10^{-12}$ C^2/Nm^2, the nanorod radius $r = 5.4$ nm, the nanorod length $l = 31.2$ nm, and we approximate the dielectric constant of the stabilizing layer as $\varepsilon = 2.7$.[12] Hence, these single-particle junctions present a 30 meV Coulomb blockade to charge transport.

To probe the extent to which the Coulomb blockade dictates the transport properties of these interconnects, we have measured and performed detailed analyses of the temperature-dependent I-V profiles of three interconnects. Those of a representative 500 μm long interconnect are shown in Fig. 4(a) for temperatures between 50 K and 300 K; while ohmic at room temperature, a voltage threshold V_t to charge transport becomes apparent below 225 K (dashed line) and increases in magnitude as the temperature is further reduced. This transition to nonlinear I-V profiles at reduced temperatures is expected when the conductance is Coulomb blockade limited; we have observed such transitions in 12 different wires. The V_t of the low-temperature I-V profiles shown in Fig. 4(a) were determined by locating the intersection between the line describing the ohmic portion of each profile above 0.035 μA and the voltage axis. The inset of Fig. 4(a) depicts the linear V_t versus T data, from which $V_t(T=0) = 3.83$ V was determined. In the absence of any thermal assistance, the applied bias must exceed $V_t(0)$ in order for current to flow through this interconnect.

Converting the I-V profiles shown in Fig. 4(a) to conductance (G)-voltage profiles, where $G = I/V$, shows that the profiles vary more weakly with voltage as the temperature increases, and that the conductance increases strongly with temperature. These G-V profiles are displayed across the 0–3 V region in Fig. 4(b). To analyze this behavior, we fit the G-V profiles to a simple model for the conductance:[13]

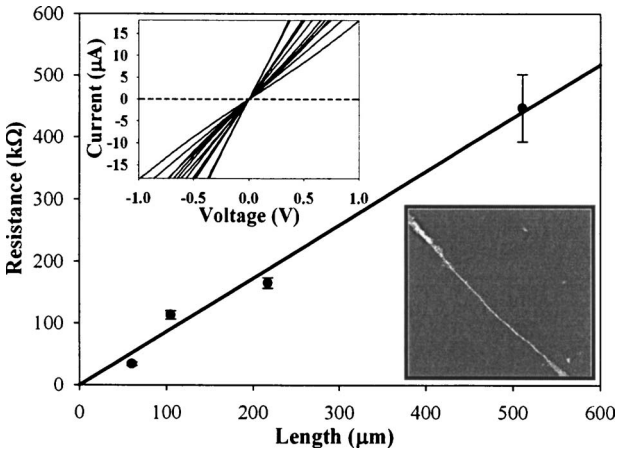

FIG. 2. Interconnect resistance vs length, measured at 300 K. The upper inset depicts I-V profiles of 15 different 60 μm long interconnects. The lower inset depicts a scanning electron micrograph of a gold nanorod interconnect.

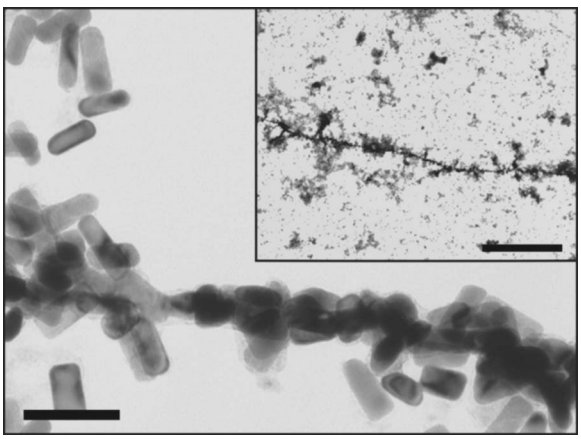

FIG. 3. Transmission electron micrographs of an interconnect dielectrophoretically assembled from the Au rods. The inset depicts a 10 μm segment of a typical interconnect (2 μm scale bar). The main panel shows an enlarged view of the right-central portion of this interconnect (50 nm scale bar).

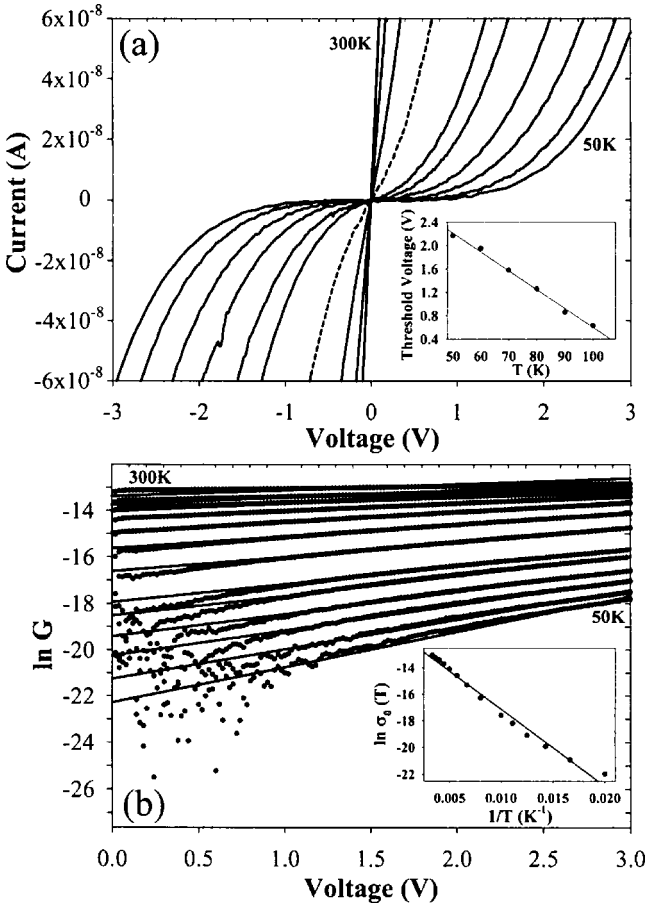

FIG. 4. (a) The *I-V* profiles of a 500 μm long interconnect for a series of temperatures. The dashed line denotes 225 K. The inset shows the voltage threshold vs temperature. (b) The conductance-voltage profiles for temperatures between 50 K and 300 K. The inset depicts the temperature dependence of the conductance at 0 V.

$G=\sigma_o(T)\exp[(eV)/(N_b k_B T)]$, where V is the voltage applied across the interconnect, N_b is the number of barriers along the length of the interconnect, $k_B T$ is the thermal energy, and $\sigma_o(T)$ is the conductance at 0 V. If electrons were to experience significant barriers to charge transport between all nanorods along the entire length of this interconnect, N_b would approximate 500 000 nm/31.2 nm $\sim$ 16 000. We determined N_b though a global fitting procedure in which a single value for N_b was chosen that best satisfied the voltage dependence of all 15 conductance profiles, and treated $\sigma_o(T)$ as the only adjustable parameter. Figure 4(b) shows that qualitative agreement between the model and the measured profiles of the 500 μm wire was attained for $N_b=150\pm30$, two orders of magnitude smaller than the value expected for charge transport between individual unfused nanorods. This result suggests that the nanorods undergo extensive fusing during interconnect formation. Supporting this finding, the TEM images in Fig. 3 are consistent with interparticle fusing, and we have detected analogous behavior in interconnects composed of CdS nanoparticles.[6] Knowledge of N_b and $V_t(0)$ enables calculation of the average magnitude of an individual barrier in the 500 μm wire: $E_b=eV_t(0)/N_b \sim 26$ meV. This barrier height is in good agreement with the charging energies of a 30 nm nanorod, $E_c \sim 30$ meV, suggesting that the Coulomb blockade is the primary barrier to charge transport in these interconnects.

To confirm this interpretation, we plot the natural log of the fit-extracted values for $\sigma_o(T)$ versus T^{-1} in the inset of Fig. 4(b) and find that the natural log of the conductance decreases linearly with T^{-1}. This Arrhenius behavior is expected for systems in which the primary mode of conduction is electronic tunneling onto a mesoscopic island that sits at a higher energy than the neighboring segments.[14] The 574 K slope of this plot indicates that an activation energy E_a of 50 meV is associated with transport onto these islands. This energy barrier falls within a factor of 2 of both E_c and E_b. Moreover, the analyses of the other two interconnects investigated in this study yielded values for E_a and E_b that fall within a factor of 4 of E_c. Given the approximate nature of the dielectric constant in the E_c calculation and the uncertainty in N_b in the E_b calculation, the agreement is acceptable. Hence, this work, based on reproducible data from lithographically fabricated electrode arrays, demonstrates the significance of the Coulomb blockade in the activated transport of dielectrophoretic interconnects. The ability to produce such wires will facilitate the development of innovative electronic devices, such as variable capacitors that require Coulomb blockade-exhibiting materials.[15]

The work was partially supported by the National Science Foundation (NER 0304413) and Oklahoma EPSCoR (EPS-132354). Additionally, the authors acknowledge the lithographic mask design by Sharmila Rajendran, the fabrication of the electrode-arrays by Yuguang Zhao, and the custom-milled chip mounts by Mike Lucas.

[1] H. A. Pohl, *Dielectrophoresis* (Cambridge University Press, Cambridge, UK, 1978).
[2] K. D. Hermanson, S. O. Lumsdon, J. P. Williams, E. W. Kaler, and O. D. Velev, Science **294**, 1082 (2001).
[3] A. Bezryadin, R. M. Westervelt, and M. Tinkham, Appl. Phys. Lett. **74**, 2699 (1999).
[4] L. A. Nagahara, I. Amlani, J. Lewenstein, and R. K. Tsui, Appl. Phys. Lett. **80**, 3826 (2002).
[5] R. Kretschmer and W. Fritzsche, Langmuir **20**, 11797 (2004).
[6] B. Ozturk, I. Talukdar, and B. N. Flanders, Appl. Phys. Lett. **86**, 183105 (2005).
[7] T. K. Sau and C. J. Murphy, Langmuir **20**, 6414 (2004).
[8] M. B. Mohamed, Z. L. Wang, and M. A. El-Sayed, J. Phys. Chem. A **103**, 10255 (1999).
[9] I. Giaever and H. R. Zeller, Phys. Rev. Lett. **20**, 1504 (1968).
[10] J. Lambe and R. C. Jaklevic, Phys. Rev. Lett. **22**, 1371 (1969).
[11] T. Kleimann, M. Sassetti, B. Kramer, and A. Yacoby, Phys. Rev. B **62**, 8144 (2000).
[12] J. G. Hou, B. Wang, J. Yang, X. R. Wang, Q. Zhu, and X. Xiao, Phys. Rev. Lett. **86**, 5321 (2001).
[13] D. Yu, C. Wang, B. L. Wehrenberg, and P. Guyot-Sionnest, Phys. Rev. Lett. **92**, 216802 (2004).
[14] M. Amman, R. Wilkins, E. Ben-Jacob, P. D. Maker, and R. C. Jaklevic, Phys. Rev. B **43**, 1146 (1991).
[15] P. Seneor, N. Lidgi, J. Carrey, H. Jaffres, F. NguyenVanDau, A. Friederich, and A. Fert, Europhys. Lett. **65**, 699 (2004).